Carbon 166 (2020) 284–290

Contents lists available at ScienceDirect

Carbon

journal homepage: www.elsevier.com/locate/carbon

Highly-dispersed cobalt clusters decorated onto nitrogen-doped carbon nanotubes as multifunctional electrocatalysts for OER, HER and ORR

Xingwei Zhou [a, 1], Xin Liu [a, 1], Jiahao Zhang [a], Cai Zhang [a], Seung Jo Yoo [b], Jin-Gyu Kim [b], Xianyu Chu [a], Chao Song [a], Peng Wang [c], Zhenzhen Zhao [a], Dabing Li [d], Wei Zhang [a, e, f, *], Weitao Zheng [a, **]

[a] Key Laboratory of Mobile Materials MOE, And School of Materials Science & Engineering, And Electron Microscopy Center, And International Center of Future Science, Jilin University, Changchun, 130012, China
[b] Electron Microscopy Research Center, Korea Basic Science Institute, Daejeon, 34133, South Korea
[c] State Key Laboratory of Superhard Materials, Jilin University, Changchun, 130012, China
[d] State Key Laboratory of Luminescence and Applications, Changchun Institute of Optics, Fine Mechanics and Physics, Chinese Academy of Sciences, Changchun, 130033, China
[e] Wuhan National Laboratory for Optoelectronics, Huazhong University of Science and Technology, Wuhan, 430074, China
[f] IKERBASQUE, Basque Foundation for Science, Bilbao, 48013, Spain

ARTICLE INFO

Article history:
Received 2 February 2020
Received in revised form
12 May 2020
Accepted 13 May 2020
Available online 18 May 2020

ABSTRACT

Preventing agglomeration and corrosion of metal electrocatalysts at nanoscale is crucial for electrochemical energy conversion, such as fuel cell and overall water splitting, where all the oxygen evolution reaction (OER), hydrogen evolution reaction (HER) and oxygen reduction reaction (ORR) are the core. Herein, an effective strategy is developed for preparing multifunctional self-supporting electrocatalysts with uniformly distributed cobalt nanoparticles and clusters. Benefiting from good electrical conductivity and multiple active sites, the trifunctional self-supporting catalyst free from stacking and aggregating exhibits excellent OER and HER activities with an overpotential of 270 and 110 mV to obtain a current density of 10 mA cm^{-2} in alkaline media. The ORR performance was tested in 0.1 M KOH solution with a half-wave potential of ~0.80 V and a limiting current density of ~ −4.8 mA cm^{-2}. Our finding provides an opportunity for the rational design of multifunctional and highly-efficient self-supporting electrocatalysts towards the integration of electrochemical energy conversion.

1. Introduction

The urgent demand for clean energy due to the inadequacy of fossil fuels and environmental issues has facilitated the wide investigation on sustainable energy conversion and storage systems (e.g., fuel cells, metal-air batteries and electrochemical water splitting) [1,2]. Meanwhile, the catalysts towards oxygen evolution reaction (OER), hydrogen evolution reaction (HER) and oxygen reduction reaction (ORR) play a crucial role in these processes, which determine the rate of electrochemical reactions by enhancing the kinetics and reducing overpotentials [3–10]. However, the scarcity, limited lifetime and high cost of precious metal resources, acting as commonly used catalysts for optimum performance, severely restrict their applications in large-scale industrial production. Hence, it is a great challenge to design and synthesize non-precious catalysts with low cost, high activity and long lifetime, which can replace precious catalysts towards a full play of all the OER, HER and ORR [11–13].

To date, non-precious metal catalysts (e.g., transition metals and their sulfides, phosphides) and non-metal catalysts (mainly carbon-based materials) have attracted great interest in electrochemical reactions, among which transition-metal-catalysts (Fe, Co and Ni)

* Corresponding author. Key Laboratory of Mobile Materials MOE, And School of Materials Science & Engineering, And Electron Microscopy Center, And International Center of Future Science, Jilin University, Changchun, 130012, China.
** Corresponding author.
E-mail addresses: weizhang@jlu.edu.cn (W. Zhang), wtzheng@jlu.edu.cn (W. Zheng).
[1] Authors contributed equally to this work.

https://doi.org/10.1016/j.carbon.2020.05.037
0008-6223/

have exhibited impressive electrocatalytic performance among OER, HER and ORR [14–17]. Transition metal-nitrogen-doped carbon-based (TM-N-C) porous nanomaterials have attracted widespread attention due to their lower cost and better performance [18,19]. Carbon materials encapsulated with nanoparticles prevent the accumulation of nanoparticles and improve the conductivity of electrocatalysts by offering the tuning electronic structure and coordination environment [20]. Such capsuling feature can effectively maintain the nanoparticles stability and inhibit their aggregation. Thus, TM-N-C catalysts enable affording the optimum ORR, OER and HER catalytic performance under alkaline conditions, which is attributed to the formation of considerable active sites by the integration of Co and N species, as well as synergistic effect [21–24]. Traditional catalysts always need binders, which leads low conductivity and the derived reduction of electrochemical activity [25,26]. The self-supporting electrocatalysts are desired as facile manufacture and stable binder-free electrodes [27]. Commonly, carbon paper (CP) and carbon cloth are used as self-supporting substrates [28], as well as foamed nickel [29] and copper [30], benefited from their good conductivity and large specific surface area [31]. Otherwise, the conventional drop-casting methods as commonly adopted ex-situ synthesis approaches tend to result in insufficient bonding between the catalysts and substrates, thereof a possible peeling of the catalysts [32]. Beyond that, tremendous efforts have been made to develop highly-efficient catalysts for the integration of OER, HER and ORR, but few of them package the significant improvement of performances as trifunctional catalysts [33]. Therefore, the development of a highly-efficient, stable and economical self-supporting multifunctional catalyst is crucial for renewable fuel cells, rechargeable metal-air batteries and water splitting.

Herein, we successfully synthesized a self-architected structure of carbon nanotubes encapsulated with cobalt nanoparticles and ultra-dispersed nanoclusters, merited by exsolution and aggregation of cobalt atoms on the surface of metal organic framework (MOF) assembled on a CP substrate, which can be directly used as an trifunctional electrocatalyst for OER, HER, ORR. Our work paves the facile route for preparing self-supporting and multifunctional electrocatalysts.

2. Experimental

2.1. Materials

Melamine and dimethylimidazole were purchased from the Sinopharm Chemical Reagent Co., Ltd. Cobalt nitrate hexahydrate was purchased from Aladdin Co., Ltd. (China). All chemicals used in this experiment were at analytical grades.

2.2. Catalyst synthesis

5 ml of ethanol and 5 g of melamine were mixed and stirred to form a 1 g/ml melamine slurry, and the slurry was placed in a graphite boat.

2.2.1. Synthesis of MCP

582 mg of cobalt nitrate hexahydrate and 1.3 g of dimethylimidazole were dissolved in 25 ml of deionized water respectively, then magnetically stirred for 0.5 h, recorded as A and B solutions. The A solution was poured quickly into the B solution. The carbon paper was placed in the obtained mixed solution, and kept at room temperature for 4 h.

2.2.2. Synthesis of Co/CNT/MCP

Melamine slurry in a graphite boat and MCP were laid in the axial direction along the tube furnace, and heated to 850 °C for 1 h (heating rate 1.8 °C min^{-1}) in a nitrogen flow. After cooling, the Co/CNT/MCP-850 was obtained. Considering the influence of temperatures, the above experiment was carried out at 800–900 °C.

2.3. Physical characterizations

The X-ray diffraction (XRD) patterns are characterized on a Bruker D8 with CuKα ray of λ = 0.15418 nm and a measured angle range of 5–80°. A scanning electron microscope (SEM, Hitachi SU8010) was applied. And transmission electron microscopy (TEM), Energy filtered TEM (EFTEM, i.e., electron energy loss spectroscopy (EELS) elemental mapping) and high-resolution TEM (HRTEM) images were recorded using electron microscopes (JEM-2100F and JEM-ARM 1300S). Raman spectroscopy was performed on Labram HR Evolution (HORIBA, 514 nm) adopted with a linear background subtraction. Surface chemical status of catalysts were detected by using X-ray photoelectron spectroscopy (XPS) (ESCALAB-250).

2.4. Electrochemical measurements

Electrochemical measurements were performed at room temperature (25 °C) using a conventional three-electrode system in conjunction with a CHI-660e electrochemical workstation (CHI Instruments, Shanghai, China). The specific operations were illustrated in Supporting Information in detail.

3. Results and discussion

The synthesis process of the catalyst is shown in Fig. 1 and the photograph of as-synthesized catalyst is given in Fig. S1. Melamine was heated to sublime and diffuse with air flow in a tubular furnace under argon (Ar) atmosphere; then it was cracked and reacted on the surface of MOF blades as carbon and nitrogen sources. Simultaneously, the triangle MOF blades in situ plated on the carbon paper (MCP, Fig. S2a) started to collapse and cobalt atoms were exsolved as Co nuclei, growing into ~30 nm Co nanoparticles or ~3 nm Co nanoclusters. Co nanoparticles acting as seeds catalyzed the generation of considerable N-doped carbon nanotubes (CNTs) (Fig. S2b), where Co nanoclusters were ultra-dispersed on the walls of CNTs at 800–1000 °C (annealed MCP without melamine shown in Fig. S3). Considering the effect of temperature on catalytic performance, we conducted the synthesis procedure at annealed temperatures from 800 to 900 °C with an interval of 50 °C. The fabricated catalysts were recorded as Co/CNT/MCP-800, Co/CNT/MCP-850 and Co/CNT/MCP-900, respectively.

As shown in Fig. 2a, CNTs with uniform diameters of ~30 nm are heavily arranged on the collapsed MOF blades upon a CP substrate, leading to a hierarchical structure. Co nanoparticles are embedded at the bottom and middle of CNTs, indicating that CNTs should be formed from the thermal diffusion of Co particles. And it was also observed that these CNTs present a bamboo-shape in Fig. 2b and 2e. In addition, the HRTEM image (Fig. 2c) demonstrate that (111) crystal plane of Co nanoparticles with a lattice fringe of 0.205 nm and (002) crystal plane of graphitic carbon. The Co nanoclusters of ~3 nm are identified from the CNTs walls, which are marked with white circles in Fig. 2d. Furthermore, based on electron energy loss spectroscopy (EELS) elemental mapping (Fig. 2e), it can be seen that carbon and nitrogen elements are homogeneously distributed throughout the CNTs. That is, a successful N-doping contributes to the formation of bamboo-shape CNTs. And cobalt is distributed on the surfaces of CNTs, besides concentrated in Co nanoparticles at the bottom and middle of CNTs. Obviously, the existence of ultra-dispersed Co nanoclusters was confirmed in accordance with our HRTEM observation (Fig. 2d). Co nanoclusters may be induced and

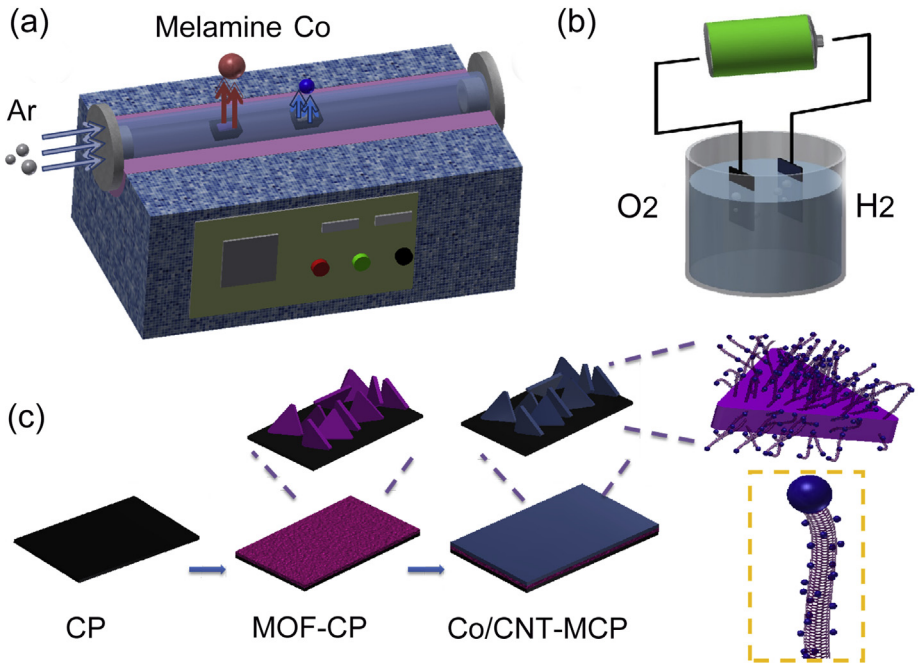

Fig. 1. Schematic illustration for the synthesis of Co/CNT/MCP: a) fabrication device and water electrolyzer. b) the proposed synthesis mechanism. (A colour version of this figure can be viewed online.)

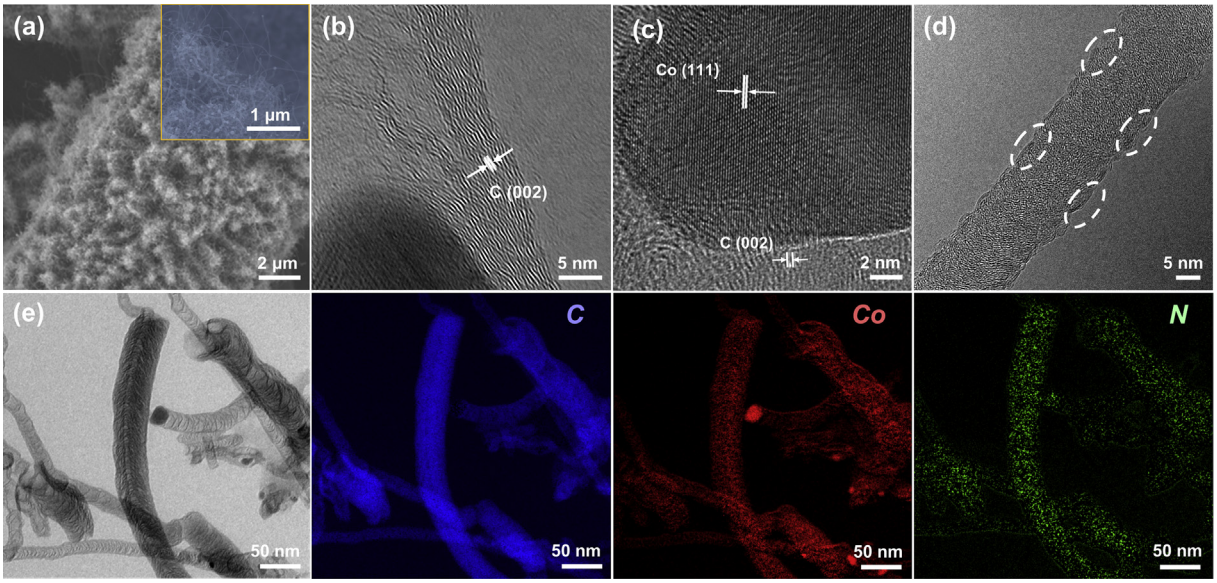

Fig. 2. a) SEM images of Co/CNT/MCP-850 with the inset of magnified one. b) TEM images of Co/CNT/MCP-850 and c) HRTEM image showing one Co nanoparticle encapsulated in graphitic carbon layers. d) HRTEM image of Co/CNT/MCP-850. e) EFTEM image series of Co/CNT/MCP-850 (C, Co and N). (A colour version of this figure can be viewed online.)

dispersed onto the CNT surfaces, while the cobalt nanoparticles are diffusing to form the CNTs assisted by the Co exsolution. For a comparison, we also prepared a sample of MCP annealed without the addition of melamine. It can be seen that considerable Co particles are deposited on the MOF blades (Fig. S3), proving that the formation of the CNTs is indeed due to Co exsolution from the MOF blades.

XRD measurements were performed to determine the crystal structure of the prepared materials, as shown in Fig. S4. The diffraction peak at 26.3° is attributed to the (002) crystal plane of the graphitic carbon from CNTs [34], and the peak at 44.2° is assigned to the (111) crystal plane of cobalt [35], which are in agreement with our HRTEM images. The rest diffraction peaks of Co metal are not significant, and it is correlated with the dominating graphitic carbon. As displayed in Fig. S5, the Raman spectra show visible bands associated with G and D bands of carbon at 1580 and 1350 cm^{-1}, respectively [36]. The relative intensity between D and G bands (I_D/I_G) corresponds to the degree of disordered carbon structure. And the I_D/I_G values of Co/CNT/MCP-800, Co/CNT/MCP-850 and Co/CNT/MCP-900 are calculated as 0.918, 0.88 and 0.908 respectively. That is, Co/CNT/MCP-850 presents a higher degrees of graphitization, corresponding to a less-defective nanotube structure [37]. The surface chemical composition of the synthesized catalysts was further analyzed by XPS. And the XPS full survey

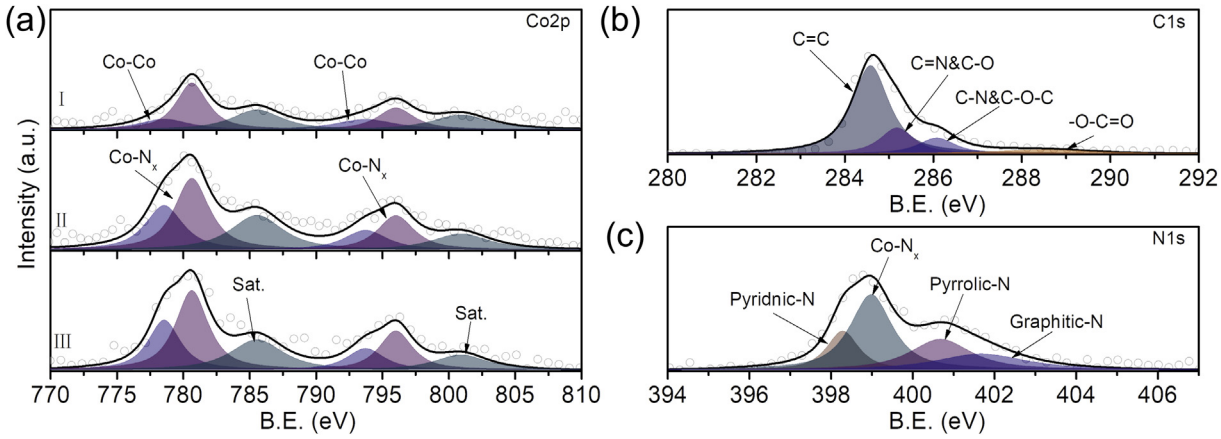

Fig. 3. a) High-resolution XPS spectra for Co2p, (I) Co/CNT/MCP-800, (II) Co/CNT/MCP-850, (III) Co/CNT/MCP-900. b) High-resolution XPS spectrum for C1s and c) N1s of Co/CNT/MCP-850. (A colour version of this figure can be viewed online.)

reveals the presences of C, N and Co elements in Co/CNT/MCP-850 catalyst (Fig. S6).

The XPS Co2p spectra of Co/CNT/MCP catalysts under three temperatures (Fig. 3a) show the multiple peaks. It indicates that Co exhibits more than one valence state. Fitting the Co2p spectrum, 1) the high-resolution spectra of Co2p3/2 and Co2p1/2 peaks are located at 778.8 and 793.8 eV; 2) the peaks at 780.7 and 796.1 eV are assigned to Co-N_x bonds, proved as activity sites for ORR and HER; 3) the other two peaks at 785.6 eV and 801.0 eV are correlated to satellite peaks [38]. The intense Co-N_x peaks in the Co/CNT/MCP-850 and Co/CNT/MCP-900 catalysts are obviously higher. Thus, a larger amount of Co-N_x sites were formed, beneficial for the high

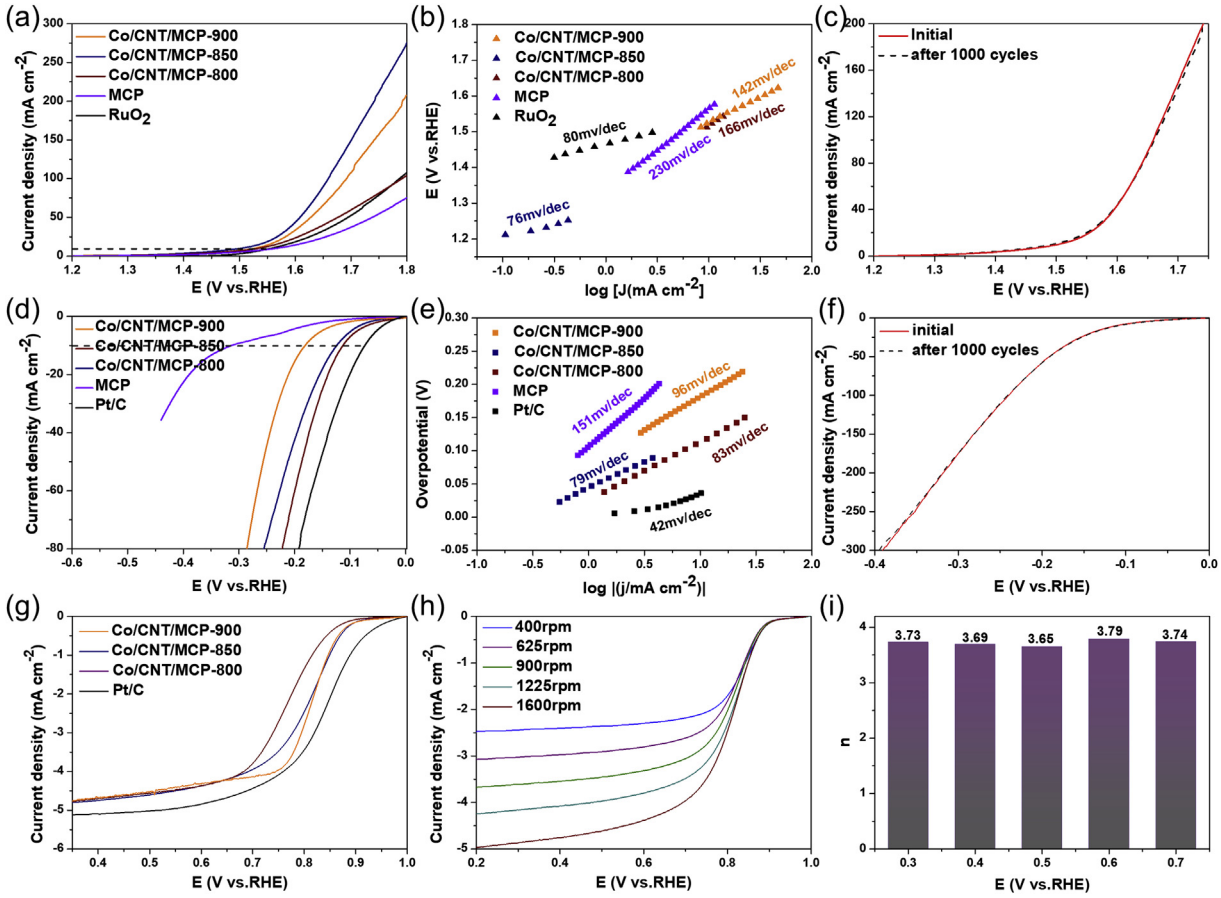

Fig. 4. OER, HER, ORR performances of Co/CNT/MCP-800, Co/CNT/MCP-850, Co/CNT/MCP-900 electrocatalysts and the corresponding noble metal catalysts. OER performance: a) OER LSV curves. b) Tafel plots of OER. c) Comparison of OER LSV curves of Co/CNT/MCP-850 catalyst before and after 1000 CV cycles. **HER performance**: d) HER LSV curves. e) Tafel plots of HER. f) Comparison of HER LSV curves of Co/CNT/MCP-850 electrocatalyst before and after 1000 cycles. **ORR performance**: g) ORR LSV curves. h) ORR LSV curves of Co/CNT/MCP-850 at different rotating speed in O_2-saturated 0.1 M KOH solution. i) Electron transfer number of Co/CNT/MCP-850 under various potentials based on the K–L plots. (A colour version of this figure can be viewed online.)

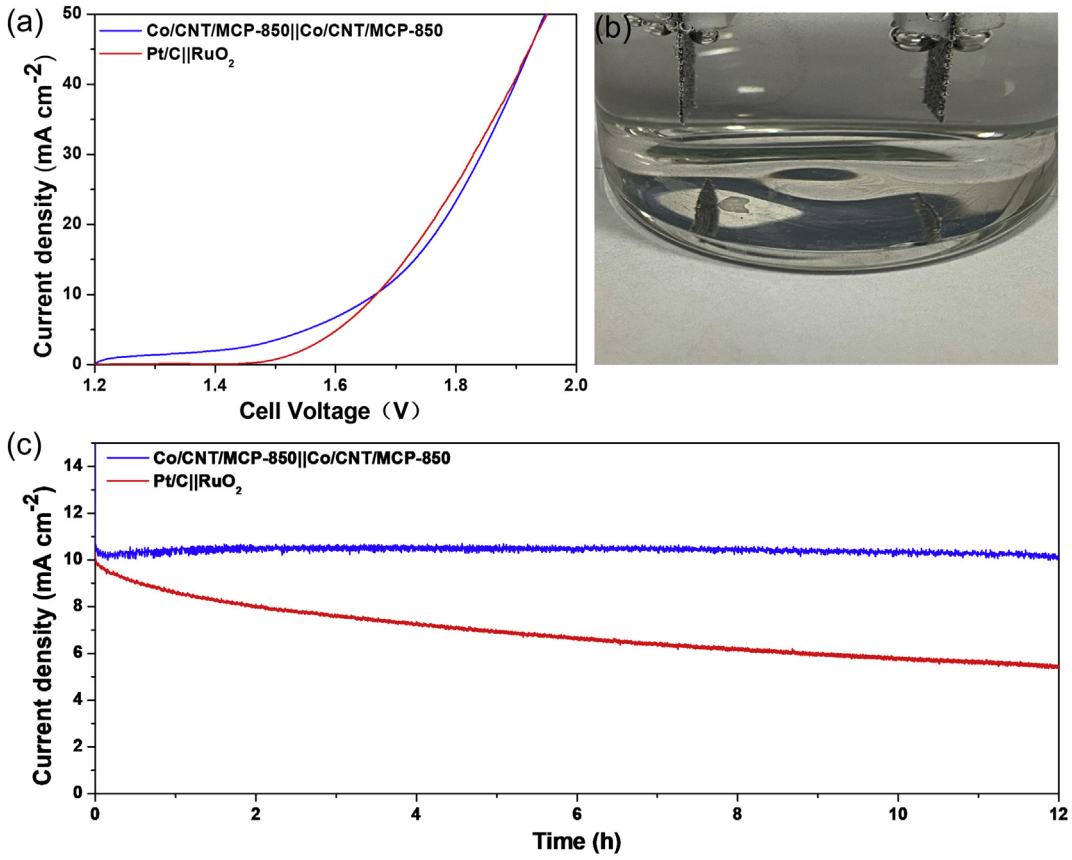

Fig. 5. a) Polarization curves for overall water splitting. b) Photograph of the electrolyzer for water splitting. c) Stability test for Co/CNT/MCP-850||Co/CNT/MCP-850 and Pt/C||RuO_2 catalysts. (A colour version of this figure can be viewed online.)

activity of catalysts. And it might be caused by the Co nanoclusters ultra-dispersed on the N-doped CNT walls, as the small sized Co nanoclusters contribute to high active surface areas, i.e., large amounts of Co-N_x bonds could be formed. From the C1s spectrum shown in Fig. 2b, four species of C peaks are characterized as C═C (284.6 eV), C—N (285.2 eV), C—O (286.1 eV) and O═C—OH (288.5 eV) [39]. In addition, Fig. 3b shows that the N1s spectrum exhibiting the peaks at 397.4, 398.7, 400, and 401.1 eV correspond to pyridinic N, Co-N_x, pyrrolic N, and graphitic N [40], further confirming the successful bonding of N to cobalt. The high content (3.3%, calculated on the basis of N atomic ratio) of Co-N_x as active sites owing to ultra-dispersive Co nanoclusters should be critical for high performance, enhancing the kinetics and reducing the overpotential [29]. Besides, N-doped CNTs encapsulated with Co nanoparticles exhibit excellent conductivity, providing facile routes for electrons transfer.

The catalytic properties of the as-prepared catalysts toward OER were demonstrated by establishing a standard three-electrode apparatus in 1.0 M KOH solution saturated with N_2. Fig. 4a shows the OER linear sweep voltammetry (LSV) curves for Co/CNT/MCP-800, Co/CNT/MCP-850, Co/CNT/MCP-900, MCP and commercial RuO_2 catalysts at a scan rate of 5 mV s^{-1} at room temperature. The Co/CNT/MCP-850 catalyst exhibits excellent OER catalytic activity with an outstanding performance of merely 270 mV to drive a current density of 10 mA cm^{-2} (E_{10} = 1.50 V), which is even much lower than RuO_2 catalysts (E_{10} = 1.55 V) and those state-of-the-art trifunctional catalysts (Table S1). The Tafel slope values indicating the kinetics of OER are calculated from the LSV curves (Fig. 4b). The Co/CNT/MCP-850 catalyst shows a smaller value of 79 mV dec^{-1} compared with other catalysts (Co/CNT/MCP-800 of 166 mV dec^{-1}, Co/CNT/MCP-900 of 142 mV dec^{-1}, and RuO_2 of 80 mV dec^{-1}), illustrating that the Co/CNT/MCP-850 performs a faster OER kinetics. In addition, to explore the inherent catalytic activity of the as-prepared catalysts, the electrochemical surface area (ECSA) of the different catalysts was also measured. The cyclic voltammograms (CV) curves for as-prepared catalysts have been demonstrated in Figs. S7a–c. As shown in Fig. S7d, Co/CNT/MCP-850 possesses the largest electric double layer capacitance (C_{dl}) value of 105 mF cm^{-2} calculated based on CV curves, which is higher than Co/CNT/MCP-800 (82 mF cm^{-2}) and Co/CNT/MCP-900 (51 mF cm^{-2}). The results indicate that the Co/CNT/MCP-850 catalyst exhibits a largest active area to expose more active sites, responsible for the significant performance towards OER. Furthermore, Co/CNT/MCP-850 catalyst has been proved to be very stable for OER. As shown in Figure S8a, the current density only drops 8% after 12 h reaction, closely correlated with the excellent electrochemical stability dependent on the unique in situ synthesized 3D structure of N-doped carbon-coated metal particles.

The HER performance of as-prepared catalysts and noble catalyst was also examined in a 1.0 M KOH solution saturated with oxygen, with MCP sample as the contrast. As shown in Fig. 4d, the HER curve of Co/CNT/MCP-850 catalyst reached a current density of 10 mA cm^{-2} at 110 mV and a current density of 100 mA cm^{-2} at 202 mV. As expected, Co/CNT/MCP-850 (Fig. 4e) shows a smaller Tafel slope (79 mV dec^{-1}) than other catalysts (Co/CNT/MCP-800 of 83 mV dec^{-1} and Co/CNT/MCP-900 of 96 mV dec^{-1}), benefited for an improved kinetic process towards HER. Hence, the remarkable performance for HER of Co/CNT/MCP-850 catalyst is very close to the commercial Pt/C catalyst with the 74 mV to drive a current density of 10 mA cm^{-2} and the Tafel slop of 42 mV dec^{-1}. Moreover,

the stability of Co/CNT/MCP-850 is critical for HER. As shown in Fig. 4f, the electrochemical performance of Co/CNT/MCP-850 is almost unchanged after 1000 cycles. And the catalytic performance did not decrease significantly (only ~1%) after 12 h current-time (I-t) test (Fig. S8b), revealing the superior catalytic performance and cycle stability of Co/CNT/MCP-850.

Also, the ORR performance was measured. As shown in Fig. 4g, in accordance with the aforementioned results, Co/CNT/MCP-850 exhibited improved ORR performance than other catalysts of Co/CNT/MCP-800 and Co/CNT/MCP-900 (Fig. S9), which is very approximate to the commercial Pt/C catalyst. The onset potential of Co/CNT/MCP-850 is 0.94 V, and the half-wave potential is 0.80 V, merely 36 mV lower than commercial Pt/C with the onset potential of 0.836 V. At a rotation rate of 1600 rpm, a current density of 4.8 mA cm^{-2} was derived as the limiting current (Fig. 4h). The electron transfer number for ORR was calculated to be 3.7 as an average value based on the Koutecky–Levich (K-L equation) at variable rotation rates (from 400 to 1600 rpm) with the linearity from 0.3 to 0.7 V (Fig. 4i and S9). It indicates that the a four-electron transfer process occurs in the catalyzed ORR by the synthesized catalysts. Furthermore, the corresponding Tafel slope of the catalysts are given in Fig. S10, illustrating a smaller value of 90 mV dec^{-1} for Co/CNT/MCP-850 than Co/CNT/MCP-800 (115 mV dec^{-1}) and Co/CNT/MCP-900 (105 mV dec^{-1}), while the Tafel slope of commercial Pt/C catalyst is 75 mV dec^{-1}. Therefore, the Co/CNT/MCP-850 catalyst affords an optimum ORR electrocatalyst property, slightly less than the commercial Pt/C catalyst.

Considering the excellent catalytic performance and long-term durability of the Co/CNT/MCP-850 catalyst for HER and OER, we tested the activity of overall water splitting in 1 M KOH using Co/CNT/MCP-850 catalysts for both the anode and cathode in a two-electrode system. Industrial electrodes with commercial Pt/C catalyst as the cathode and RuO_2 catalyst as the anode were performed for comparison. As shown in Fig. 5a, the Co/CNT/MCP-850 catalyst exhibited a superior overall water splitting performance to the commercial Pt/C and RuO_2 industrial electrodes, driving a current density of 10 mA cm^{-2} at 1.66 V. The photograph of water splitting electroyzer is shown in Fig. 5b. In addition, the durability of the catalysts for overall splitting water was investigated, while the water electrolysis process was performed at a current density of 10 mA cm^{-2} for 12 h, with a potential decay of only 1% for Co/CNT/MCP-850 catalysts (Fig. 5c). In contrast, the long-term stability of Pt/C||RuO_2 is not satisfactory, with a potential decay of 50% after 12 h. In general, Co/CNT/MCP-850 catalyst has excellent stability as a whole water splitting catalyst.

4. Conclusions

In summary, we successfully synthesized a carbon nanotube based trifunctional catalyst supported on carbon paper by using a facile in situ approach. Cobalt nanoparticles are exsolved from MOF blades during annealing and then the formation of N-doped CNT was promoted via Co nanoparticles catalyzing the thermally diffusing carbon and nitrogen sources. Simultaneously, the Co nanoclusters are highly dispersed on the CNT walls. The issue of agglomeration and corrosion of metal nanoparticles are well addressed by this unique uniform distribution of cobalt nanoparticles and cobalt clusters. Moreover, the catalyst affords excellent electrocatalyst performance towards the integration of OER, HER and ORR in alkaline solutions, provided with fast kinetics and long-term stability. The optimal Co/CNT/MCP-850 catalyst electrode exhibits promisingly high performance in the overall water slitting test. Our work can be a fingerprinting reference for the strategy of metal thermal diffusion technology to prepare self-supporting multifunctional electrocatalysts towards large-scale industrial production.

Declaration of competing interest

The authors declare that they have no known competing financial interests or personal relationships that could have appeared to influence the work reported in this paper.

CRediT authorship contribution statement

Xingwei Zhou: Conceptualization, Investigation, Writing - original draft. **Xin Liu:** Conceptualization, Writing - original draft. **Jiahao Zhang:** Investigation. **Cai Zhang:** Resources. **Seung Jo Yoo:** Investigation. **Jin-Gyu Kim:** Investigation. **Xianyu Chu:** Investigation. **Chao Song:** Investigation. **Peng Wang:** Investigation. **Zhenzhen Zhao:** Resources. **Dabing Li:** Resources. **Wei Zhang:** Conceptualization, Writing - review & editing. **Weitao Zheng:** Conceptualization, Writing - review & editing.

Acknowledgments

We gratefully acknowledge the financial support provided by the National Natural Science Foundation of China (51872115, 51932003), 2020 International Cooperation Project of the Department of Science and Technology of Jilin Province (20200801001GH), Program for the Development of Science and Technology of Jilin Province (20190201309JC), Jilin Province/Jilin University Co-Construction Project Funds for New Materials (SXGJSF2017-3, Branch-2/440050316A36), the Project supported by State Key Laboratory of Luminescence and Applications (KLA-2020-05), the Open Project Program of Wuhan National Laboratory for Optoelectronics (2018WNLOKF022), Program for JLU Science and Technology Innovative Research Team (JLUSTIRT, 2017TD-09), the Fundamental Research Funds for the Central Universities JLU, "Double-First Class" Discipline for Materials Science & Engineering.

Appendix A. Supplementary data

Supplementary data to this article can be found online at https://doi.org/10.1016/j.carbon.2020.05.037.

References

[1] I. Roger, M.A. Shipman, M.D. Symes, Nat. Rev. Chem 1 (2017), 0003.
[2] D. Zu, H. Wang, S. Lin, G. Ou, H. Wei, S. Sun, H. Wu, Nano Res 12 (2019) 2150–2163.
[3] A. Serov, M. Padilla, A.J. Roy, P. Atanassov, T. Sakamoto, K. Asazawa, H. Tanaka, Angew Chem. Int. Ed. Engl. 53 (2014) 10336–10339.
[4] M. Shao, Q. Chang, J.P. Dodelet, R. Chenitz, Chem. Rev. 116 (2016) 3594–3657.
[5] H. Zhang, Y. Liu, T. Chen, J. Zhang, J. Zhang, X.W.D. Lou, Adv. Mater. (2019), e1904548.
[6] D. Zhao, K. Sun, W.-C. Cheong, L. Zheng, C. Zhang, S. Liu, X. Cao, K. Wu, Y. Pan, Z. Zhuang, B. Hu, D. Wang, Q. Peng, C. Chen, Y. Li, Angew. Chem. 131 (2019) 2–11.
[7] S. Huang, Y. Meng, Y. Cao, S. He, X. Li, S. Tong, M. Wu, Appl. Catal. B Environ. 248 (2019) 239–248.
[8] C. Zhang, W. Zhang, S. Yu, D. Wang, W. Zhang, W. Zheng, M. Wen, H. Tian, K. Huang, S. Feng, J.J. Bentzen, ChemElectroChem 4 (2017) 1269–1273.
[9] C. Zhang, W. Zhang, N.E. Drewett, X. Wang, S.J. Yoo, H. Wang, T. Deng, J.-G. Kim, H. Chen, K. Huang, S. Feng, W. Zheng, ChemSusChem 12 (2019) 1000–1010.
[10] C. Zhang, S. Yu, Y. Xie, W. Zhang, K. Zheng, N.E. Drewett, S.J. Yoo, Z. Wang, L. Shao, H. Tian, J.-G. Kim, W. Zheng, Carbon 149 (2019) 370–379.
[11] L. Gao, X. Li, Z. Yao, H. Bai, Y. Lu, C. Ma, S. Lu, Z. Peng, J. Yang, A. Pan, H. Huang, J. Am. Chem. Soc. 141 (2019) 18083–18090.
[12] T. Zhang, M.-Y. Wu, D.-Y. Yan, J. Mao, H. Liu, W.-B. Hu, X.-W. Du, T. Ling, S.-Z. Qiao, Nano Energy 43 (2018) 103–109.
[13] P. Yu, F. Wang, T.A. Shifa, X. Zhan, X. Lou, F. Xia, J. He, Nano Energy 58 (2019) 244–276.
[14] Y. Lian, W. Yang, C. Zhang, H. Sun, Z. Deng, W. Xu, L. Song, Z. Ouyang, Z. Wang, J. Guo, Y. Peng, Angew. Chem. Int. Ed. 59 (2020) 286–294.

[15] C. He, T. Bo, B. Wang, J. Tao, Nano Energy 62 (2019) 85–93.
[16] J. Lu, Z. Tang, L. Luo, S. Yin, P. Kang Shen, P. Tsiakaras, Appl. Catal. B Environ. 255 (2019), 117737.
[17] Y. Men, P. Li, J. Zhou, G. Cheng, S. Chen, W. Luo, ACS Catal. 9 (2019) 3744–3752.
[18] Y. Zhu, G. Chen, X. Xu, G. Yang, M. Liu, Z. Shao, ACS Catal. 7 (2017) 3540–3547.
[19] S. Liu, Z. Wang, S. Zhou, F. Yu, M. Yu, C.-Y. Chiang, W. Zhou, J. Zhao, J. Qiu, Adv. Mater. 29 (2017), 1700874.
[20] L. Zhang, S. Zhu, S. Dong, N.J. Woo, Z. Xu, J. Huang, J.-K. Kim, M. Shao, J. Electrochem. Soc. 165 (2018) J3271–J3275.
[21] J. Zhu, L. Hu, P. Zhao, L.Y.S. Lee, K.Y. Wong, Chem. Rev. 120 (2020) 851–918.
[22] D.U. Lee, P. Xu, Z.P. Cano, A.G. Kashkooli, M.G. Park, Z. Chen, J. Mater. Chem. 4 (2016) 7107–7134.
[23] M. Zhang, Q. Dai, H. Zheng, M. Chen, L. Dai, Adv. Mater. 30 (2018), 1705431.
[24] Z. Chen, R. Wu, Y. Liu, Y. Ha, Y. Guo, D. Sun, M. Liu, F. Fang, Adv. Mater. 30 (2018), e1802011.
[25] W. Hong, C. Jian, G. Wang, X. He, J. Li, Q. Cai, Z. Wen, W. Liu, Appl. Catal. B Environ. 251 (2019) 213–219.
[26] D. Yan, Y. Li, J. Huo, R. Chen, L. Dai, S. Wang, Adv. Mater. 29 (2017), 1606459.
[27] Z. Yang, C. Zhao, Y. Qu, H. Zhou, F. Zhou, J. Wang, Y. Wu, Y. Li, Adv. Mater. 31 (2019), e1808043.
[28] J.X. Feng, J.Q. Wu, Y.X. Tong, G.R. Li, J. Am. Chem. Soc. 140 (2018) 610–617.
[29] Z. Chen, Y. Song, J. Cai, X. Zheng, D. Han, Y. Wu, Y. Zang, S. Niu, Y. Liu, J. Zhu, X. Liu, G. Wang, Angew Chem. Int. Ed. Engl. 57 (2018) 5076–5080.
[30] C.-T. Dinh, A. Jain, F.P.G. de Arquer, P. De Luna, J. Li, N. Wang, X. Zheng, J. Cai, B.Z. Gregory, O. Voznyy, B. Zhang, M. Liu, D. Sinton, E.J. Crumlin, E.H. Sargent, Nat. Energy 4 (2018) 107–114.
[31] B. Qiu, M. Xing, J. Zhang, Chem. Soc. Rev. 47 (2018) 2165–2216.
[32] J. Zhang, K. Xiao, T. Zhang, G. Qian, Y. Wang, Y. Feng, Electrochim. Acta 226 (2017) 113–120.
[33] Y. Wu, X. Tao, Y. Qing, H. Xu, F. Yang, S. Luo, C. Tian, M. Liu, X. Lu, Adv. Mater. 31 (2019), e1900178.
[34] X. Miao, D. Sun, X. Zhou, Z. Lei, Chem. Eng. J. 364 (2019) 208–216.
[35] T. Liu, Y. Pang, M. Zhu, S. Kobayashi, Nanoscale 6 (2014) 2447–2454.
[36] X. Zhao, X. He, B. Chen, F. Yin, G. Li, Appl. Surf. Sci. 487 (2019) 1049–1057.
[37] Q. Yang, Z. Xiao, D. Kong, T. Zhang, X. Duan, S. Zhou, Y. Niu, Y. Shen, H. Sun, S. Wang, L. Zhi, Nano Energy 66 (2019), 104096.
[38] D.R. Deng, F. Xue, Y.J. Jia, J.C. Ye, C.D. Bai, M.S. Zheng, Q.F. Dong, ACS Nano 11 (2017) 6031–6039.
[39] X. Ji, B. Liu, X. Ren, X. Shi, A.M. Asiri, X. Sun, ACS Sustain. Chem. Eng. 6 (2018) 4499–4503.
[40] S. Jing, L. Zhang, L. Luo, J. Lu, S. Yin, P.K. Shen, P. Tsiakaras, Appl. Catal. B Environ. 224 (2018) 533–540.